Journal Name

ARTICLE TYPE

Cite this: DOI: 10.1039/xxxxxxxxxx

Electrospray deposition of structurally complex molecules revealed by atomic force microscopy

Antoine Hinaut,*[a] Tobias Meier,[a] Rémy Pawlak,[a] Sara Feund,[a] Res Jöhr,[a] Shigeki Kawai,[b] Thilo Glatzel,[a] Silvio Decurtins, [c] Klaus Müllen,[d] Akimitsu Narita,[d] Shi-xia Liu[c] and Ernst Meyer*[a]

Received Date
Accepted Date

DOI: 10.1039/xxxxxxxxxx

www.rsc.org/journalname

Advances in organic chemistry allow the synthesis of large, complex and highly functionalized organic molecules having potential applications in optoelectronics, molecular electronics and organic solar cells. Their integration into devices as individual components or highly ordered thin-films is of paramount importance to address these future prospects. However, conventional sublimation techniques in vacuum are usually not applicable since large organic compounds are often non-volatile and decompose upon heating. Here, we prove by atomic force microscopy and scanning tunneling microscopy, the structural integrity of complex organic molecules deposited onto an Au(111) surface using electrospray ionisation deposition. High resolution AFM measurements with CO-terminated tips unambiguously reveal their successful transfer from solution to the gold surface in ultra-high vacuum without degradation of their chemical structures. Furthermore, the formation of molecular structures from small islands to large and highly-ordered self-assemblies of those fragile molecules is demonstrated, confirming the use of electrospray ionisation to promote also on-surface polymerization reactions of highly functionalized organic compounds, biological molecules or molecular magnets.

1 INTRODUCTION

A promising route to built-up small functional systems at the nanometer scale relies on the spontaneous assembly of molecules with chemical functionality on atomically clean surfaces prepared in ultra-high vacuum (UHV) [1–3]. Common to all these approaches is the creation of nanostructured molecular patterns, based on growth mechanism with specific chemical motifs favouring regio-selective intermolecular interactions [4–6]. The art of innovation in synthetic chemistry has meanwhile reached a high level of complexity in preparing extended and structurally intricate functional molecules [7,8]. However, their use in UHV environment is restricted by their thermal stability. Increase of the molecular weight further increases the sublimation temperature leading to fragmentation. Consequently alternative deposition techniques are required.

Electrospray deposition (ESD) [9,10] is thus an ideal alternative to address this issue since it allows the transfer of molecules from the solution onto a surface under vacuum conditions. The setup consists of a linear differential pumping system where small solvent droplets are ionized using high voltages and directed towards the sample maintained in vacuum condition. By minimizing the contamination caused by solvent molecules with ESD [9–19] or by using more sophisticated methods like Electrospray Ion beam deposition (ES-IBD) [20–28] possibly equipped with soft landing devices, it is possible to deposit molecules and large biomolecules on various substrates such as metals, oxides or bulk insulators. The deposited molecules were observed in real-space using atomic force microscopy (AFM) and scanning tunneling microscopy (STM) techniques either as single molecules or self-assemblies [18,19,24]. Therefore, ESD allows to deposit such large or fragile molecules, with the restriction that they are soluble, and might open future avenues into the development of molecular-based devices.

Scanning probe microscopy techniques are powerful tools to characterize the molecular properties at surfaces while the electrospray deposition technique widely broadens the range of accessible molecular structures, with a diversity of functionalities. The recent advances in high-resolution AFM imaging have further enabled the characterization of those molecular systems at

[a] Department of Physics, University of Basel, Klingelbergstrasse 82, CH 4056 Basel, Switzerland. Tel: +41 (0)61 207 3724; E-mail: antoine.hinaut@unibas.ch; ernst.meyer@unibas.ch
[b] International Center for Materials Nanoarchitectonics, National Institute for Materials Science, 1-1, Namiki, Tsukuba, Ibaraki 305-0044, Japan.
[c] Department of Chemistry and Biochemistry, University of Bernn Freiestrasse 3, CH 3012 Bern, Switzerland.
[d] Max Planck Institute for Polymer Research, Ackermannweg 10, 55128 Mainz, Germany

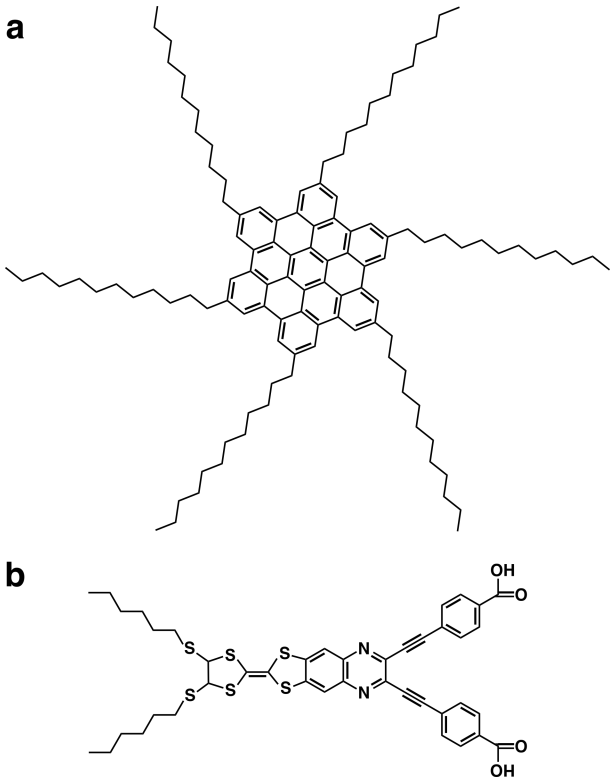

Fig. 1 Chemical structures of the $HBC6C_{12}$ and TTF-dye molecules. (a) Hexadodecylhexabenzocoronene ($HBC6C_{12}$). (b) Fused TTF-quinoxaline molecule with benzoic acid and alkyl end groups (TTF-dye). Scale bar ≃1 nm.

the intramolecular level arriving at a fundamental understanding into their physical properties [29]. High-resolution AFM imaging either obtained at room temperature (RT) or at low temperature (LT) can nowadays elucidate the chemical structure of those organic adsorbates which is an asset to confirm their integrity under the ESD method [19,29–34].

Here we report the electrospray deposition on Au(111) of two prototypical precursors: the hexadodecyl-hexa-peri-hexabenzocoronene ($HBC6C_{12}$), consisting of a large aromatic core and six long alkyl chains (Fig. 1a) and the tetrathiafulvalene-based dye (TTF-dye), a fused electron donor-acceptor molecule (Fig. 1b). Combining AFM experiments with sub-molecular resolution at RT (300 K), we show that the on-surface $HBC6C_{12}$ assembly is governed by alkyl-alkyl interactions leading to the formation of achiral domains in analogy to the liquid-solid interface [35–37]. By decreasing the substrate temperature to 5 K, AFM measurements further show that the $HBC6C_{12}$ assembly undergoes a structural phase transition resulting in two enantiomeric assemblies due to the prochirality of the molecule. Using TTF-dye molecules, we further demonstrate that fragile chemical moieties such as tetrathiafulvalene or benzoic acid end groups attached to a carbon backbone can also be deposited, without degradation, on surfaces. Although containing alkyl chains, the TTF-dye assembly is there driven by the H-bond interaction between carboxylic acid end groups rather then the interdigitation of alkyl groups leading to small molecule assemblies.

2 METHODS

Sample preparation. Au(111) single crystals purchased from Mateck GmbH were prepared in ultra-high vacuum conditions by cycles of Ar^+ sputtering (≈ 1 kV for 10 min) and annealing at 750 K. With such procedure, atomically flat surfaces are obtained with large terraces separated by atomic steps.

$HBC6C_{12}$ molecule. The molecule was synthesized with the following procedure [38].

TTF-dye molecule. TTF-dye molecule was prepared according to literature [39].

Room-Temperature nc-AFM. Room temperature (RT) nc-AFM experiments are conducted in our home built AFM microscope operating in an ultra-high vacuum. Commercially available Si cantilevers (Nanosensors PPP-NCL, $k_c \simeq 33$ N/m) are used as force sensor. They are annealed to 400 K for 1 hour, and tips are subsequently cleaned by Ar^+ sputtering (680 eV for 90 s). NcAFM with the first flexural resonance (f_1) is used to obtain surface topography. The resonance frequency shifts are demodulated by digital phase-locked loops (PLL) (Nanonis Dual-OC4).

Low-Temperature STM/AFM. Low temperature STM/AFM experiments were realized with a low-temperature microscope (Omicron Nanotechnology GmbH) operated at 5 K with Nanonis RC5 electronics and based on a tuning fork sensor in the qPlus configuration (stiffness $k = 1800$ N/m, resonance frequency $f = 25$ kHz, at 5 K, oscillation amplitude of $A = 50$ pm). The STM experiments were conducted in the constant-current mode. The bias voltage is given by the potential of the sample referred to the tip. The differential conductance measurements were acquired with the standard lock-in technique (frequency $f_{mod} = 532$ Hz, voltage modulation $A_{mod} = 9$ mV).

Electrospray Deposition. ESD is based on the Electrospray ionization [40,41]. The Molecularspray setup is connected to the UHV preparation chamber of the systems [11,19]. After the spray is formed in air, highly charged droplets [42,43] enter by a capillary into the differential pumping system composed of the three chambers separated by leak orifices. The droplets beam is directed to the sample and during the path through the differential pumping system, a loss of the solvent is obtained. Nevertheless, all species introduced in vacuum are directed to the surface and a fine control of ESD is required to limit the pollution on the sample. In such condition, homogeneous coverage is obtained on the sample. $HBC6C_{12}$ and TTF-dye molecules are dissolved in a mixture of toluene and methanol (ratio of 4:1). Solvents are high purity chromasolv from Sigma-Aldrich. Solution is introduced in the electrospray device via a syringe pump with a rate of maximum $60 \cdot \mu L \cdot hour^{-1}$ connected via capillary to the emitter. A bias of typically 1.5 kV, sometimes adjusted to maintain spray quality, is then applied in between the solution and the entrance capillary to create the spray. Time of spray deposition is 10 min for the $HBC6C_{12}$ and 5 min for the TTF-dye molecule. During the deposition the sample is at room temperature and the base pressure of the chamber increases from $1 \cdot 10^{-10}$ mbar up to 10^{-7} mbar. The spray deposition is tuned with the quality of the spray jet and plume, with the measurement of the pressure in the deposition chamber as well as with change in current

measurement on the sample.

3 RESULTS and DISCUSSION

Van der Waals interaction to stabilize HBC6C$_{12}$ assemblies.

To illustrate the limitation of thermal deposition of large molecules in UHV, the example of molecular networks stabilized by van der Waals interactions between long peripheral alkyl chains is well-suited[36,44–46]. From STM studies, it is well established that, at liquid-solid interfaces, those molecular assemblies are governed by the interdigitation of long alkyl chains[24,35–37,47,48]. However, molecules with such long and numerous alkyl chains are difficult to evaporate under UHV due to the high molecular weight combined to the strong π-π interactions that would request elevated temperature where molecules are generally degraded by breaking of their alkyl chains. Previous studies of large polycyclic aromatic hydrocarbon (PAH) molecule were performed at the liquid solid interface using STM[35,49–51]. However, in UHV, only the HBC core is thermally stable and studied at surfaces[52,53]. In our case, the HBC6C$_{12}$ molecule (Fig. 1a) contains six dodecyl chains (C$_{12}$) attached to the HBC core preventing its thermal evaporation without degradation.

Fig. 2a shows an AFM topography image of an as-received Au(111) surface after ESD. The image is localized on a large HBC6C$_{12}$ islands up to hundred nanometers are formed on the Au(111) surface. The gold herringbone structure is visible but no correlation with the molecular arrangement is observed. This observation indicates that the molecule-substrate interaction is rather weak (physisorption). In terms of size, the lattice parameter of the hexagonal network is $\sim$2.6 nm according real-space measurements as well as fast Fourier transforms (FFT) of the image (Fig. 2c). This is in agreement with a flat-lying interdigitated network of the HBC6C$_{12}$ molecules. Gentle annealing up to 370 K were also conducted to study possible structural changes of the molecular network but no alteration of the lattice or of the island morphology was observed after annealing.

To further study the electronic properties of this system, we also conducted experiments at lower temperature using combined STM/AFM. ESD were performed at room temperature without post annealing of the gold surface. The sample was then directly transferred to the microscope and image at 5 K. Fig. 2b shows a STM topographic image of a similar HBC6C$_{12}$ islands compared to Fig. 2a. The individuals alkyl chains are visible between the nearby HBC cores. Surprisingly, the lattice of the molecular network is slightly smaller than the one at room temperature since it measures $\sim$ 2.2 nm according to the the FFT images and real-space measurements (Fig. 2d).

The differential conductance measurement dI/dV was acquired above the HBC core of the molecules (Fig. 2e). The two resonance peaks located at -1.4 V and +1.55 V corresponds to the highest occupied molecular orbital (HOMO) and lowest unoccupied molecular orbitals (LUMO), respectively. The shoulder at -0.9 V is likely the contribution of the gold state through the molecule. These resonance peaks are in relative good agreement with previous investigations of HBC molecule without alkyl chains using photo-electron spectroscopy[54] and conductance measurements[55,56] showing HOMO and LUMO resonance peaks at -1.5 V and +1.8 V, respectively.

Atomic scale imaging of HBC6C$_{12}$ to reveal chirality.

The molecule interdigitation within the islands at room temperature is shown with high-resolution in Fig. 3a revealing a star-like shape as expected from the six-fold symmetry of the molecule (Fig. 1a). The HBC cores are imaged as bright dots surrounded by six peripheral protrusions corresponding to the alkyl chains. Each protrusions coincide with the interdigitation of pairs of alkyl chains from two neighbouring molecules as depicted in the model Fig. 3b. In such structure, each molecule adopts a star-like shape as expected in the gas phase with dodecyl chains pointing toward the center of the HBC core. The dimension of the model is also in agreement with the lattice of the molecular network obtained from the FFT image (Fig. 2c).

To get a deeper insight into the chain interdigitation at lower temperature, high-resolution AFM imaging of those islands were performed at 5 K with CO terminated tips (Fig. 3c,d). For each molecule, the HBC core is revealed similar to previous works[53] (Fig. 3d) as well as the surrounding alkyl chains (Fig. 3c). In this structure, each alkyl chain of nearby molecules are facing each other leading to a slightly different arrangement compared to the islands at RT. Indeed, the alignment has a different angle with respect to the core and the opposite chains are laterally shifted (Fig. 3f,h) compared to the the room temperature assembly (Fig. 3b). Furthermore, the HBC6C$_{12}$ molecule adopts at low temperature a chiral conformation leading to enantiomeric assemblies at the surface depicted in Fig. 3f and h. This leads to a decrease of $\sim$ 15 % of the lattice parameter due to the temperature (from 2.6 nm at 300 K to 2.2 nm at 5 K). With this compression of the network, the alkyl chains interdigitation is maximized and van der Waals interaction increases. This also suggest for the RT case that the two chiral conformation are frequently switched by large thermal energy at room temperature. Consequently the size of the network becomes larger. In addition, for LT, all molecules within a molecular domain adopts the same chiral conformation, thus leading to two enantiomeric assemblies confined at the surface[57].

Hydrogen bonding motive to stabilize TTF-dye islands.

To go a step beyond, we tackled the TTF-dye molecule, a fused electron donor-acceptor (DA) system[58]. Specifically the electron donor bearing long alkyl chains is annulated to a quinoxaline electron acceptor which is further functionalized with two benzoic acid groups (Fig.1b)[39]. Fused DA molecules show an intramolecular charge transfer upon photoexcitation leading to a wide spectral absorption range. Consequently, it is used in dye-sensitized solar cells (DSSC) exhibiting one of the highest power conversion efficiencies for TTF sensitizers[39]. The study of the structural and electronic properties of isolated electron DA molecules

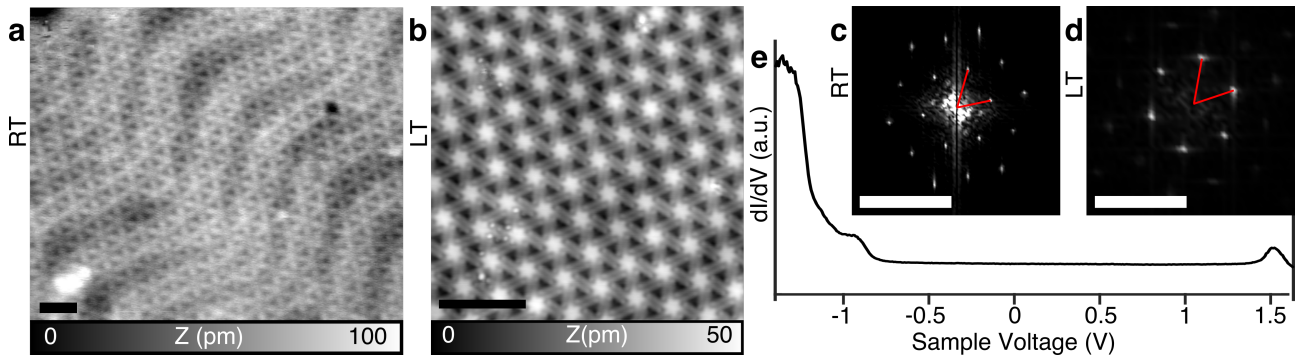

Fig. 2 RT and LT imaging of the HBC6C$_{12}$ on the Au(111) surface. (a) Large scale RT-non contact AFM topographic image of the HBC6C$_{12}$ assembly on Au(111) (f_1 = 176 kHz, Δf_1 = -50 Hz, A = 2 nm). (b) Large scale LT-STM image of the assembly, (I = 2 pA, U = -200 mV). (c,d) FFT images of Fig. a and b respectively. Lattice vectors are indicated in red. (e) Differential conductance dI/dV spectra acquired above the HBC core. Scale bar: topography: 5 nm; FFT: 1 nm^{-1}.

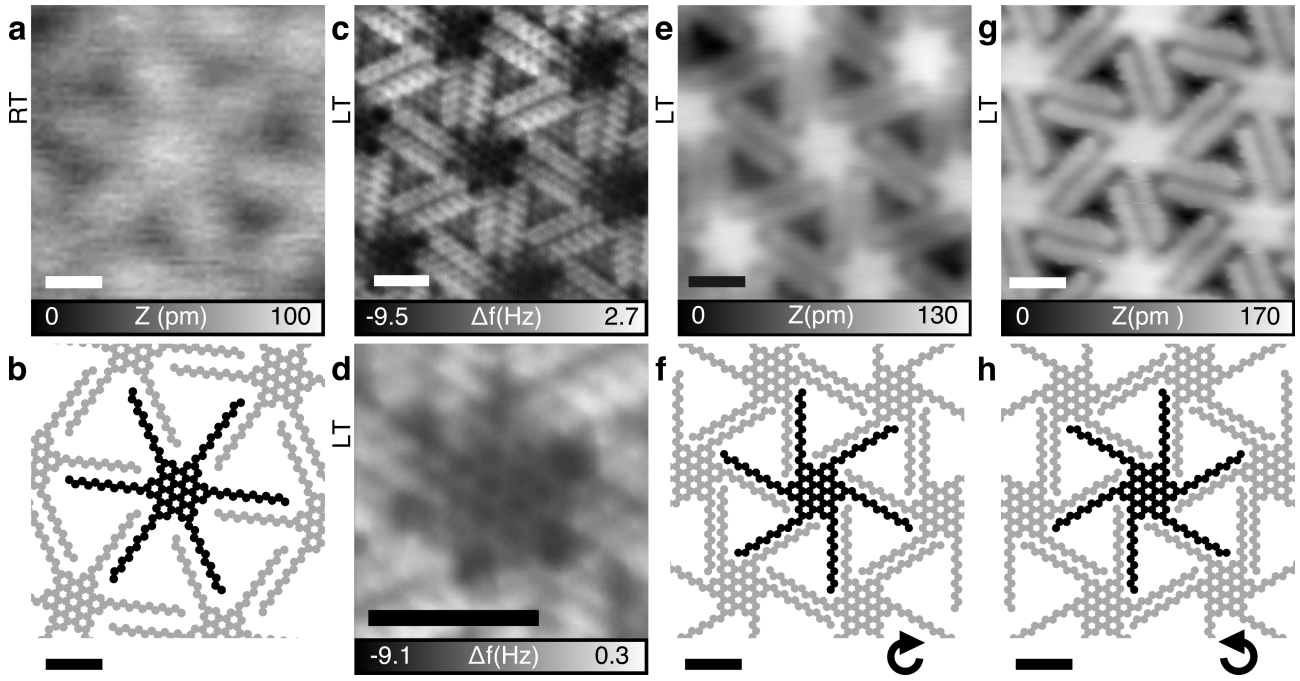

Fig. 3 High resolution imaging of the HBC6C$_{12}$ assembly on Au(111). (a) Room temperature topography nc-AFM image of molecules in a molecular island. (b) Corresponding model of the network at room temperature. (c) Low temperature constant-height AFM image with CO terminated tip. (d) Close-up image of the HBC core of the molecule. (e) and (g) STM images on molecules from two different islands showing the two enantiomer orientations. (f) and (h) are the proposed model for the molecular alignment and alkyl chains interdigitation in the two types of islands. Parameters: (a) f_1 = 176 kHz, Δf_1 = -30 Hz, A = 5 nm. (c,d) A = 40 pm, U = 0 V , (e) I = 2 pA, U = -200 mV; (g) I = 1 pA, U = -1.5 V. Scale bar is 1 nm.

has been tackled using scanning probe techniques in previous works[59–61]. For DSSC applications, to efficiently promote charge transfer from the molecule to the substrate, functional groups such as anchoring units are preferable[62]. As aforementioned, the increased weight of such molecules and the reactive components prevents its thermal evaporation in UHV. Therefore, the simplest DA molecules have been investigated at the atomic level[60,61].

Taking advantages of the ESD technique, we have deposited a complex dye molecule (Fig. 1b), containing alkyl chains and carboxyl groups on Au(111). Fig. 4a shows a STM overview image of TTF-dye molecules on the surface. The molecules assemble in small symmetric islands of three to six molecules. Occasionally, some TTF-dye molecules fragments are also found at the surface that lead to the formation of asymmetric islands like in Fig. 4b. The driving motive for the TTF-dye molecule assembly in small islands is visible by resolving their chemical structure using constant-height AFM images with CO terminated tips (Fig. 4d). In the assembly, the carboxylic acid end groups face each other whereas the alkyl chains are at the periphery of the island. The alkyl chains appear as zig-zag structure in the AFM images and show a higher frequency shift Δf value compared to the rest of the molecule (Fig. 4d). This observation suggests that they are closer to the tip than the backbone of the molecule, likely because alkyl chains are very mobile and tend to move during the scans. Furthermore, the phenyl rings as well as the quinoxaline moieties, are observed flat-lying in the AFM image. The two in-

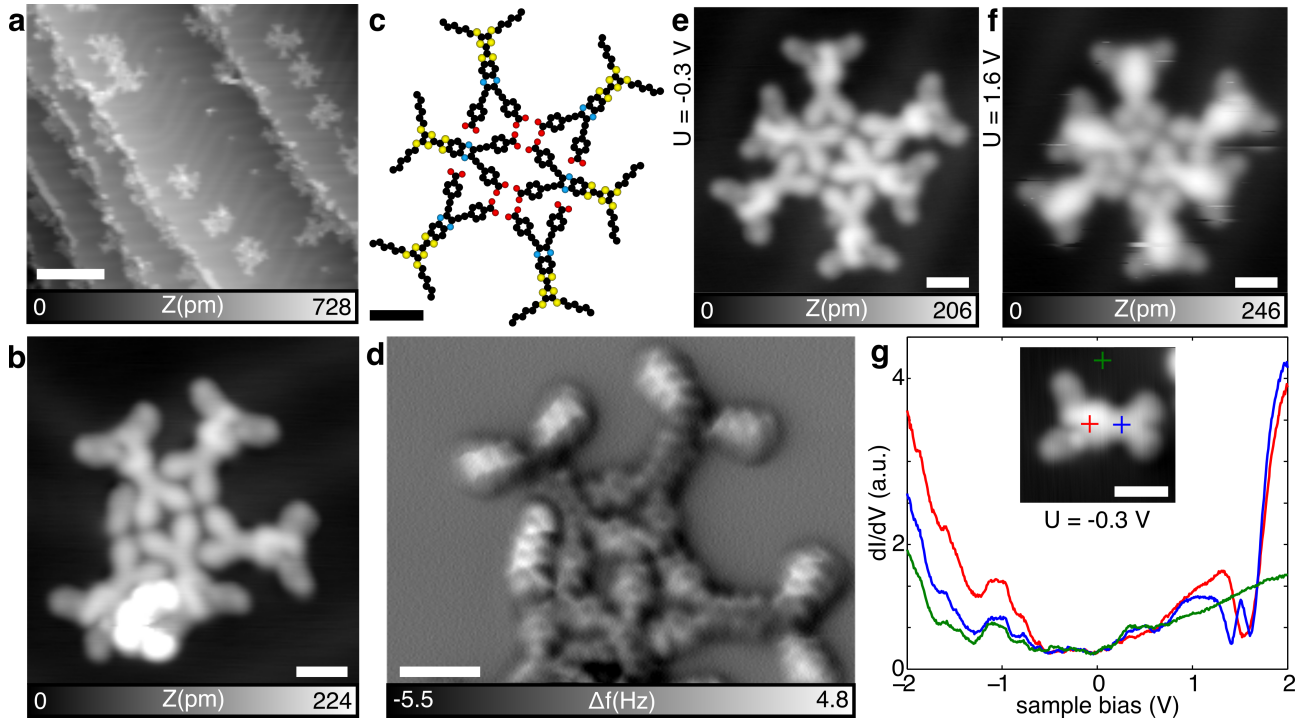

Fig. 4 Islands of TTF-dye molecules on Au(111).(a) STM overview image showing the assembling of TTF-dye molecules in small islands (I = 10 pA, U = -0.5 V, scale bar 10 nm). In some of the islands, fragments are observed after ESD deposition. (b,d) STM image of such an island (I = 5 pA, U = -0.3 V) and corresponding constant height AFM image with a CO terminated tip (U = 0 V). (c) Model of the arrangement of the TTF-dye molecules representing the island in image (e) experimentally observed by STM (I = 5 pA, U = -0.3 V). (f) STM image of the same island at I = 1 pA, U = 1.6 V. (g) STS spectra of TTF-dye. The tip position is indicated by the cross in red (TTF moiety), in blue (quinoxaline moiety) and in green (Au(111) substrate) in the inset. (b-g) the scale bars are 1 nm. All images and spectra were recorded at T = 5 K.

ner molecules face each other (Fig. 4c). One of the carboxylic acid groups, in the four outer molecules, is always linked to those of the inner molecules and the other carboxylic acid group points towards a nitrogen atom of the pyrazine unit, both induced by hydrogen bonding[63]. The bonding motive of the molecular assemblies is shown in Fig. 4e. The number of TTF-dye molecules in islands does not exceed six and is limited by the number of regioselective hydrogen binding between molecules in contrast to what observed with molecular assemblies with only alkyl chains. This also shows that the hydrogen bonding interaction are stronger than all van der Waals interaction resulting from full alkyl chains.

Differential conductance spectra of the molecules were recorded above a TTF-dye molecule at the TTF donor (red), the quinoxaline acceptor (blue) and at the gold substrate (green). For negative biases, only resonances coinciding with the gold substrate are observed which prevents the assignment of the energetic position of the HOMO states of the TTF-dye molecule (Fig. 4g). For positive biases, two additional resonance peaks with respect to the substrate appear at $\sim$ 1 V for quinoxaline and 1.3 V for the TTF moiety, respectively. We attribute these peaks to the lowest unoccupied molecular orbital (LUMO) of the molecule. Scanning at positive voltages around this LUMO energy (Fig. 4f) reveals that the TTF-dye molecule appears larger on the TTF moiety. Since the LUMO is expected to be at the quinoxaline location[39], the electronic alignment seems to be mediated by the metallic substrate. Nevertheless, the intrinsic structure and electronic properties are preserved thorough ESD deposition.

4 CONCLUSIONS

By using the ESD technique, structurally complex molecules with functional groups were deposited in UHV. High resolution AFM images unambiguously identified the chemical structure of the $HBC6C_{12}$ and TTF-dye precursors proving that the chemical functionalities are maintained at the surface. In both cases, the deposition leads to molecular assemblies over the gold surface governed either by hydrogen bondings between carboxylic acid groups or van der Waals interactions between peripheral alkyl chains. Interestingly, we show that $HBC6C_{12}$ assemblies undergo a chiral phase transition by decreasing the temperature from 300 K to $\sim$ 5 K also inducing a molecular network lattice reduction. At such low temperature, the flexible alkyl chains promote the formation of a pro-chiral molecule conformation leading to the formation of two enantiomeric domains at the surface which are not present at room temperature. We also extended the study of electro-sprayed fragile precursors using a prototypical donor-acceptor compound, the TTF-dye molecule. In that case, small assemblies are also observed. Although containing alkyl chains, the assembly is there driven by the H-bond interaction between carboxylic acid end groups rather then the interdigitation of alkyl groups. The combination of ESD and AFM opens the scope for studies on the atomic level of large molecular precursors with attractive properties such as intriguing biradical ground state. It allows the investigation of large molecules where functionalized groups are spatially separated. Furthermore,

novel on-surface chemical reactions become accessible because they are not prevented due to low thermal activation energy during the standard deposition technique of thermal evaporation.

Conflict of interest

There are no conflicts to declare.

ACRONYMS

ESD, electro spray deposition; ESI, electro spray ionization; STM, scanning tunneling microscopy; AFM, atomic force microscopy; STS, scanning tunneling spectroscopy; HOMO, highest occupied molecular orbital; LUMO, lowest unoccupied molecular orbital.

AUTHORS CONTRIBUTION

A.H., R.P. and E.M. planned the project. A.H. developed the spray apparatus and performed all spray depositions. A.H. performed the AFM measurements at RT. T.M. and R.P. performed the STM/AFM measurements at LT. A.N. and K.M. synthesized the $HBC6C_{12}$ molecule and S.X.L. and S.D. synthesized the TTF-dye molecule. A.H., T.M. and R.P. analysed the data. A.H. and T.M. co-wrote the paper with the help of R.P. All authors discussed on the results and revised the manuscript.

ACKNOWLEDGEMENTS

We acknowledge financial support from the Swiss National Science Foundation (SNSF), the Swiss Nanoscience Institute (SNI), the Cost-Action MP1303, the Japan Society for the Promotion of Science (JSPS) KAKENHI Grant Number 15K21765, and the Max Planck Society.

References

1 J. V. Barth, G. Costantini and K. Kern, *Nature*, 2005, **437**, 671–679.

2 N. Kocić, P. Weiderer, S. Keller, S. Decurtins, S.-X. Liu and J. Repp, *Nano Lett.*, 2015, **15**, 4406–4411.

3 N. Kocić, X. Liu, S. Chen, S. Decurtins, O. Krejčí, P. Jelínek, J. Repp and S.-X. Liu, *J. Am. Chem. Soc.*, 2016, **138**, 5585–5593.

4 J. Cai, P. Ruffieux, R. Jaafar, M. Bieri, T. Braun, S. Blankenburg, M. Muoth, A. P. Seitsonen, M. Saleh, X. Feng, K. Müllen and R. Fasel, *Nature*, 2010, **466**, 470–473.

5 L. Grill, *J. Phys.: Condens. Matter*, 2008, **20**, 053001.

6 N. A. A. Zwaneveld, R. Pawlak, M. Abel, D. Catalin, D. Gigmes, D. Bertin and L. Porte, *J. Am. Chem. Soc.*, 2008, **130**, 6678–6679.

7 A. Narita, X.-Y. Wang, X. Feng and K. Müllen, *Chem. Soc. Rev.*, 2015, **44**, 6616–6643.

8 Y. Lin, Y. Li and X. Zhan, *Chem. Soc. Rev.*, 2012, **41**, 4245–4272.

9 J. C. Swarbrick, J. B. Taylor and J. N. O'Shea, *Appl. Surf. Sci.*, 2006, **252**, 5622 – 5626.

10 C. J. Satterley, L. M. A. Perdigão, A. íSaywell, G. Magnano, A. Rienzo, L. C. Mayor, V. R. Dhanak, P. H. Beton and J. N. O'Shea, *Nanotechnology*, 2007, **18**, 455304.

11 *Molecularspray*, `http://www.molecularspray.co.uk/`, 2017.

12 A. Saywell, G. Magnano, C. J. Satterley, L. M. A. Perdigão, N. R. Champness, P. H. Beton and J. N. O'Shea, *J. Phys. Chem. C*, 2008, **112**, 7706–7709.

13 A. Saywell, J. K. Sprafke, L. J. Esdaile, A. J. Britton, A. Rienzo, H. L. Anderson, J. N. O'Shea and P. H. Beton, *Angew. Chem., Int. Ed.*, 2010, **49**, 9136–9139.

14 A. Rienzo, L. C. Mayor, G. Magnano, C. J. Satterley, E. Ataman, J. Schnadt, K. Schulte and J. N. O'Shea, *J Chem Phys*, 2010, **132**, 084703.

15 A. Saywell, G. Magnano, C. J. Satterley, L. M. Perdigão, A. J. Britton, N. Taleb, M. del Carmen Giménez-López, N. R. Champness, J. N. O'Shea and P. H. Beton, *Nature Communications*, 2010, 1–8.

16 K. Handrup, V. J. Richards, M. Weston, N. R. Champness and J. N. O'Shea, *J Chem Phys*, 2013, **139**, 154708.

17 S. A. Svatek, L. M. A. Perdigão, A. Stannard, M. B. Wieland, D. V. Kondratuk, H. L. Anderson, J. N. O'Shea and P. H. Beton, *Nano Lett.*, 2013, **13**, 3391–3395.

18 P. Erler, P. Schmitt, N. Barth, A. Irmler, S. Bouvron, T. Huhn, U. Groth, F. Pauly, L. Gragnaniello and M. Fonin, *Nano Lett.*, 2015, **15**, 4546–4552.

19 A. Hinaut, R. Pawlak, E. Meyer and T. Glatzel, *Beilstein J Nanotechnol*, 2015, **6**, 1927–1934.

20 S. Rauschenbach, F. L. Stadler, E. Lunedei, N. Malinowski, S. Koltsov, G. Costantini and K. Kern, *Small*, 2006, **2**, 540–547.

21 C. Hamann, R. Woltmann, I.-P. Hong, N. Hauptmann, S. Karan and R. Berndt, *Rev. Sci. Instrum.*, 2011, **82**, 033903–6.

22 K. Steffen, Z. Deng, N. Malinowski, C. Tonnoir, A. Forment-Aliaga, N. Thontasen, G. Rinke, D. Len, V. Turkowski, T. S. Rahman, S. Rauschenbach, M. Ternes and K. Kern, *Nano Letters*, 2012, **12**, 518–521.

23 A. Bodin, R. Laloo, P. Abeilhou, L. Guiraud, S. Gauthier and D. Martrou, *Rev. Sci. Instrum.*, 2013, **84**, 095104.

24 N. Hauptmann, K. Scheil, T. G. Gopakumar, F. L. Otte, C. Schütt, R. Herges and R. Berndt, *J. Am. Chem. Soc.*, 2013, **135**, 8814–8817.

25 C. S. Kley, C. Dette, G. Rinke, C. E. Patrick, J. Čechal, S. J. Jung, M. Baur, M. Dürr, S. Rauschenbach, F. Giustino, S. Stepanow and K. Kern, *Nano Lett.*, 2014, **14**, 563–569.

26 S. Rauschenbach, M. Ternes, L. Harnau and K. Kern, *Annual Review of Analytical Chemistry*, 2016, **9**, 473–498.

27 S. Rauschenbach, G. Rinke, R. Gutzler, S. Abb, A. Albargash, D. Le, T. Rahman, M. Dürr, L. Hanau and K. Kern, *ACS Nano*, 2017, 2420–2427.

28 J.-N. Longchamp, S. Rauschenbach, S. Abb, C. Escher, T. Latychevskaia, K. Kern and H.-W. Fink, *PNAS*, 2017, **114**, 1474–1479.

29 L. Gross, F. Mohn, N. Moll, P. Liljeroth and G. Meyer, *Science*, 2009, **325**, 1110–1114.

30 R. Pawlak, S. Kawai, S. Fremy, T. Glatzel and E. Meyer, *ACS Nano*, 2011, **5**, 6349–6354.

31 O. Guillermet, S. Gauthier, C. Joachim, P. de Mendoza, T. Lauterbach and A. Echavarren, *Chem. Phys. Lett.*, 2011, **511**, 482–485.

32 S. Kawai, A. Sadeghi, X. Feng, P. Lifen, R. Pawlak, T. Glatzel, A. Willand, A. Orita, J. Otera, S. Goedecker and E. Meyer, *ACS Nano*, 2013, 9098–9105.

33 K. Iwata, S. Yamazaki, P. Mutombo, P. Hapala, M. Ondráček, P. Jelínek and Y. Sugimoto, *Nat. Commun.*, 2015, **6**, 7766.

34 F. Huber, S. Matencio, A. Weymouth, C. Ocal, E. Barrena and F. Giessibl, *Phys. Rev. Lett.*, 2015, **115**, 066101.

35 S. D. Feyter and F. C. D. Schryver, *Chem. Soc. Rev.*, 2003, **32**, 139–150.

36 K. Tahara, S. Lei, J. Adisoejoso, S. De Feyter and Y. Tobe, *Chem. Commun.*, 2010, **46**, 8507.

37 K. S. Mali, J. Adisoejoso, E. Ghijsens, I. De Cat and S. De Feyter, *Acc. Chem. Res.*, 2012, **45**, 1309–1320.

38 P. Samorí, C. D. Simpson, K. Müllen and J. P. Rabe, *Langmuir*, 2002, **18**, 4183–4185.

39 A. Amacher, C. Yi, J. Yang, M. P. Bircher, Y. Fu, M. Cascella, M. Grätzel, S. Decurtins and S.-X. Liu, *Chem. Commun.*, 2014, 6540–6542.

40 J. B. Fenn, M. Mann, C. K. Meng, S. F. Wong and C. M. Whitehouse, *Science*, 1989, **246**, 64–71.

41 J. B. Fenn, *J. Am. Soc. Mass Spectrometry*, 1993, **4**, 524–535.

42 S. J. Gaskell, *J. Mass Spectrom.*, 1997, **32**, 677–688.

43 P. Kebarle and U. H. Verkerk, *Mass Spectrom. Rev.*, 2009, **28**, 898–917.

44 J. P. Rabe and S. Buchholz, *Science*, 1991, **253**, 424–427.

45 K. Müllen, *ACS Nano*, 2014, **8**, 6531–6541.

46 S. Wickenburg, J. Lu, J. Lischner, H.-Z. Tsai, A. A. Omrani, A. Riss, C. Karrasch, A. Bradley, H. S. Jung, R. Khajeh, D. Wong, K. Watanabe, T. Taniguchi, A. Zettl, A. H. C. Neto, S. G. Louie and M. F. Crommie, *Nat. Commun.*, 2016, **7**, 13553.

47 D. X. Shi, W. Ji, X. Lin, X. B. He, J. C. Lian, L. Gao, J. M. Cai, H. Lin, S. X. Du, F. Lin, C. Seidel, L. F. Chi, W. A. Hofer, H. Fuchs and H.-J. Gao, *Phys. Rev. Lett.*, 2006, **96**, 226101.

48 B. Schuler, Y. Zhang, S. Collazos, S. Fatayer, G. Meyer, D. Pérez, E. Guitián, M. R. Harper, J. D. Kushnerick, D. Peña and L. Gross, *Chem. Sci.*, 2017, **8**, 2315–2320.

49 C. Marie, F. Silly, L. Tortech, K. Müllen and D. Fichou, *ACS Nano*, 2010, **4**, 1288–1292.

50 W. Pisula, A. Menon, M. Stepputat, I. Lieberwirth, U. Kolb, A. Tracz, H. Sirringhaus, T. Pakula and K. Müllen, *Adv Mater*, 2005, **17**, 684–689.

51 D. W. Breiby, O. Bunk, W. Pisula, T. I. Sølling, A. Tracz, T. Pakula, K. Müllen and M. M. Nielsen, *J. Am. Chem. Soc.*, 2005, **127**, 11288–11293.

52 H. Glowatzki, G. N. Gavrila, S. Seifert, R. L. Johnson, J. Räder, K. Müllen, D. R. T. Zahn, J. P. Rabe and N. Koch, *J Phys Chem C*, 2008, **112**, 1570–1574.

53 L. Gross, F. Mohn, N. Moll, B. Schuler, A. Criado, E. Guitián, D. Peña, A. Gourdon and G. Meyer, *Science*, 2012, **337**, 1326–1329.

54 H. Proehl, M. Toerker, F. Sellam, T. Fritz, K. Leo, C. Simpson and K. Müllen, *Phys. Rev. B*, 2001, **63**, 205409.

55 M. Toerker, T. Fritz, H. Proehl, R. Gutierrez, F. Großmann and R. Schmidt, *Phys. Rev. B*, 2002, **65**, 245422.

56 W.-H. Soe, H. S. Wong, C. Manzano, M. Grisolia, M. Hliwa, X. Feng, K. Müllen and C. Joachim, *ACS Nano*, 2012, **6**, 3230–3235.

57 S. Weigelt, C. Busse, L. Petersen, E. Rauls, B. Hammer, K. V. Gothelf, F. Besenbacher and T. R. Linderoth, *Nat. Mater.*, 2006, **5**, 112–117.

58 J. J. Bergkamp, S. Decurtins and S.-X. Liu, *Chem. Soc. Rev.*, 2015, **44**, 863–874.

59 C. Tao, J. Sun, X. Zhang, R. Yamachika, D. Wegner, Y. Bahri, G. Samsonidze, M. L. Cohen, S. G. Louie, T. D. Tilley, R. A. Segalman and M. F. Crommie, *Nano Lett.*, 2009, **9**, 3963–3967.

60 B. Schuler, S.-X. Liu, Y. Geng, S. Decurtins, G. Meyer and L. Gross, *Nano Lett.*, 2014, **14**, 3342–3346.

61 T. Meier, R. Pawlak, S. Kawai, Y. Geng, X. Liu, S. Decurtins, P. Hapala, A. Baratoff, S.-X. Liu, P. Jelínek, E. Meyer and T. Glatzel, *ACS Nano*, 2017, **11**, 8413–8420.

62 R. Jöhr, A. Hinaut, R. Pawlak, Ł. Zajac, P. Olszowski, B. Such, T. Glatzel, M. Muntwiler, J. J. Bergkamp, L.-M. Mateo, S. Decurtins, S.-X. Liu and E. Meyer, *J Chem Phys*, 2017, **146**, 184704.

63 M. Böhringer, K. Morgenstern, W.-D. Schneider, R. Berndt, F. Mauri, A. D. Vita, and R. Car, *Phys. Rev. Lett.*, 1999, 324–327.